

Article

Characterization of Siliceous Nodules in Western Kefalonia Island Greece: An Initial Approach to Their Formation and Diagenetic Characteristics

Paraskevi Lampropoulou ¹, Vayia Xanthopoulou ^{1,2}, Małgorzata Wojtaszek-Kalaitzidi ³, Petros Petrounias ¹, Elena Zoumpouli ^{1,4}, George Iliopoulos ¹ and Stavros Kalaitzidis ^{1,*}

¹ Department of Geology, University of Patras, 26504 Patras, Greece; p.lampropoulou@upatras.gr (P.L.); vxanthopoulou@upatras.gr (V.X.); Geo.plan@outlook.com (P.P.); elzoumpouli@upatras.gr (E.Z.); iliopoulosg@upatras.gr (G.I.)

² Laboratory of Electron Microscopy and Microanalysis, School of Natural Sciences, University of Patras, 26504 Patras, Greece

³ Institute for Chemical Processing of Coal, 41803 Zabrze, Poland; mwojtaszek@ichpw.pl

⁴ Kefalonia-Ithaca Geopark, Koutavos Environmental Center, 28100 Argostoli, Greece

* Correspondence: skalait@upatras.gr



Citation: Lampropoulou, P.; Xanthopoulou, V.; Wojtaszek-Kalaitzidi, M.; Petrounias, P.; Zoumpouli, E.; Iliopoulos, G.; Kalaitzidis, S. Characterization of Siliceous Nodules in Western Kefalonia Island Greece: An Initial Approach to Their Formation and Diagenetic Characteristics. *Minerals* **2022**, *12*, 101. <https://doi.org/10.3390/min12010101>

Academic Editors: Georgia Pe-Piper, Avraam Zelilidis and Ioannis Iliopoulos

Received: 18 November 2021

Accepted: 12 January 2022

Published: 15 January 2022

Publisher's Note: MDPI stays neutral with regard to jurisdictional claims in published maps and institutional affiliations.



Copyright: © 2022 by the authors. Licensee MDPI, Basel, Switzerland. This article is an open access article distributed under the terms and conditions of the Creative Commons Attribution (CC BY) license (<https://creativecommons.org/licenses/by/4.0/>).

Abstract: In this study, siliceous nodules from the world-famous Myrtos beach, as well as from Avithos beach, in the western flanks of Kefalonia Island in Greece are examined by means of petrographical, mineralogical, geochemical and micropaleontological methods. The objectives of this study are to characterize the textural and compositional features of the nodules, with the aim to provide an initial interpretation of their origin and their diagenetic evolution. The studied siliceous nodules are hosted within Lower Cretaceous thin-bedded limestones at Myrtos and Upper Eocene limestones at Avithos. Nodules from both areas display a characteristic concentric texture at a macroscopic and microscopic scale. They both have a dense fine-grained siliceous sedimentary fabric, composed mainly of microcrystalline or cryptocrystalline quartz and moganite with common residual calcite in the case of Avithos. These results, and in particular the shape of the nodules, along the textural and compositional characteristics, indicate different conditions of formation in the two localities, both during the early epigenetic stages, as well as later during the diagenetic processes. Myrtos nodules originated from Si-precursors deposited in a pelagic environment, going through intense Si-replacement. Avithos nodules were deposited in a more proximal environment, being influenced by a less intense silicification. Nevertheless, the higher degree of recrystallization of Avithos samples indicates a syn- or post-diagenetic tectonic activity that resulted in the circulation of geothermal fluids. The conclusions drawn from this work demonstrate the usefulness of thorough studies of siliceous nodules in order to get a more comprehensive understanding of the initial depositional conditions, as well as diagenetic pathways and processes.

Keywords: cherts; flint-like rocks; Kefalonia island; moganite; siliceous nodules

1. Introduction

Different varieties of siliceous sedimentary rocks (i.e., siliceous nodules, cherts, porcelainite, etc.) have been investigated all over the world according to their textural, sedimentological and physicochemical characteristics [1–6]. Among the siliceous sedimentary rocks the cherts are dominant, being described as siliceous hard-dense rocks consisting mainly of micro to cryptocrystalline quartz and low impurities, ranging in ages from Precambrian to Quaternary. The most common mode of origin of Si in these lithologies is either related to biogenic or hydrothermal processes [2,6,7]. Siliceous lithologies usually are hosted within carbonate rocks (e.g., limestones, chalk) as layers or as nodules, the latter after replacement of carbonate minerals by amorphous biogenetic silica under changing palaeodepositional

or diagenetic conditions [7–9]. Varieties of the siliceous nodules that display zoning of high-purity micro-layers of grey-tones are commonly termed as flints [1,10].

The increased scientific interest in siliceous rocks, either from geologists, gemologists, or archaeologists, lies in the fact that these lithotypes have been extensively used by various cultures throughout human history because of their hardness and weathering resistance. Furthermore, their systematic study provides significant information about their silica source, the palaeo-depositional conditions and the diagenetic evolution [1,3,7]. For instance, Gotze et al. [11] have shown an inverse correlation between the amount of moganite in agates with their age of formation, while Bourli et al. [3,4] have related the different sizes of siliceous nodules with redox-diagenetic zones and host rock characteristics. Nevertheless, the variety of siliceous nodules types, host rocks, the timing of formation and diagenetic pathways does not allow for a simplistic “genesis-model”, although the importance of Si-input and redox boundaries in the sea-bed subsurface play the most crucial role at the early epigenetic stages, e.g., [1,11].

Moreover, the detailed petrogeochemical evaluation of such rocks in combination with their physico-mechanical properties contributed further to the knowledge of their potential utilization. Luedtke [12] highlighted the strong relationship between mineralogical and microstructural characteristics of siliceous rocks (cherts), as well as their water content with their thermo- mechanical strength and knapping characteristics. Nevertheless, nowadays siliceous rocks are mainly used as gemstones and tumbled stones, and less for other purposes (e.g., guns, blades, ceramics, construction materials) [12].

On the other hand, archaeologists focus on the sources of chert artifacts, since these rocks played an important role in being used as tools by prehistoric communities, after knapping or heat treatments. Physicochemical characteristics (e.g., hardness, color, impurities, etc.) and macro-microtextural characteristics (e.g., shape, fracture, lustre, mineralogy, grain size, weathering phenomena) are very important criteria for researchers and related provenance studies of chert artifacts, providing significant answers about their signature, the past human techniques and culture or further information about the migration of populations and trade development [6,12–14]. However, recent studies indicated that a detailed macroscopic and petrogeochemical characterization of the siliceous stones is necessary for provenance issues to be answered [6,15]. In Greece, as in many places around the world, outcropping siliceous rocks have been studied, as well as artifacts from different regions such as Western Macedonia, Aegean area or Ionian Sea from both geological and archeological points of view [3,4,16–18].

Although siliceous nodules from Kefalonia island have been the subject of a recent study [4,18], in this article the characteristics of siliceous nodules hosted within carbonates that outcrop in Myrtos and Avithos bays, respectively (Figure 1), in the western coastal part of Kefalonia island (Greece), are presented for the first time. The objectives of this study focus on the textural and compositional features of the nodules by applying a set of optical and electron microscopical techniques, mineralogical and geochemical analyses. The aim of this initial approach is to provide a base characterization of the siliceous nodules, as well as an interpretation of their origin and diagenetic evolution.

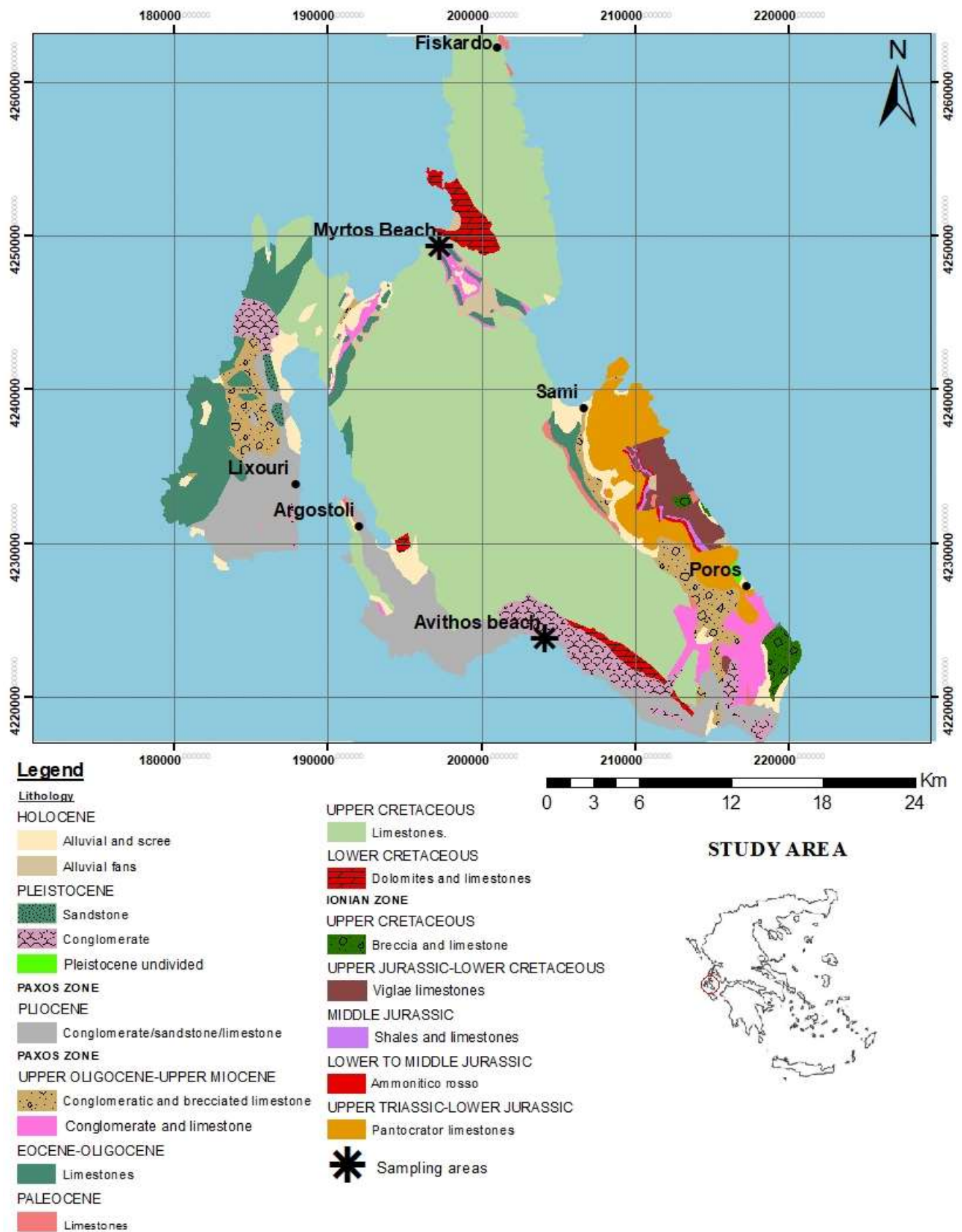


Figure 1. Geological map of Kefalonia, modified after [19].

2. Geological Setting

Kefalonia Island belongs to the Ionian Islands and lies at the external edge of the Hellenides fold-and-thrust system created in response to the Cenozoic continental collision following the closure of the Tethys Ocean [20–23]. The external Hellenides lie to the west of the Pindos thrust and are subdivided into three units: the Gavrovo, the Ionian, and the Pre-Apulian Units. The Gavrovo and the Ionian Units have been considered to represent the external large Hellenide thrust sheets emplaced onto the relatively stable Pre-Apulian autochthon, as part of the latest Hellenic orogenic events [20,24–26]. The geological structure of Kefalonia consists of two different geotectonic units (alpine formations) of the External Hellenides, with an overall NNW-SSE orientation (Figure 1).

The Pre-Apulian Unit, in the west, is the autochthonous foreland of the Hellenic fold-thrust belt, and is generally believed to have been unaffected by major shortening [20,24,26–30], covering the major part of the island. The Ionian zone appears in the southeastern part of the island, and is thrust over the Pre-Apulian Unit.

From the Triassic to the Late Cretaceous, Western Greece was part of the Apulian continental block on the southern passive margin of Tethys. Specifically, the island of Kefalonia is characterized by widely exposed Cretaceous limestones of the Pre-Apulian and Ionian Units, which were deposited at the margin of the Apulian carbonate platform. The Pre-Apulian Unit of the Kefalonia island is characterized by a continuous sequence of neritic carbonate rocks (dolomites, limestones, marly limestones), with deposition starting in the Early Cretaceous and continuing until the Late Miocene (marly sediments, often sandstones, alternating with brecciated limestones). The Ionian Unit comprises sedimentary formations ranging from Triassic evaporites to Jurassic Upper Eocene carbonate rocks, including minor chert and shale horizons, overlain by Oligocene flysch deposits [29–31]. Finally, Pliocene-Quaternary formations can be identified, which rest unconformably on the older rocks (Figure 1).

Myrtos bay is located in northwestern Kefalonia, in a transitional zone, between the northern part of Mount Aenos (Mount Agia Dynati) and the southern part of the Erissos (Kalon Oros) peninsula. The region belongs to the Pre-Apulian Unit, consisting of Upper Cretaceous limestones, Paleocene fine-bedded pelagic limestones, Eocene well bedded pelagic limestones (up to 120 m thick) including greyish to reddish chert beds, and finally Miocene marl formations. Tectonically, this area is affected by the NW-SE strike-slip reverse fault of Agia Efimia [3], since the area is still under stress. The Avithos region presents strongly tectonized and folded Eocene limestones, which are unstratified or densely bedded with bioclasts of foraminifera (*Nummulites*, *Alveolina*) and algae (*Microcodium*). The thickness of these neritic limestones does not exceed 40 m.

3. Materials and Methods

Sampling took place in outcropping carbonate cliffs at Myrtos Beach (MB, Figures 1 and 2) and Avithos Beach (AVB, Figures 1 and 3). A total of three nodules were collected from each site based on their macroscopical characteristics (i.e., shape, texture, size, and colour based on [32]). However, since the nodules displayed very similar macroscopic and petrographic features, only one sample per site was geochemically analyzed.

The MB samples derived from Myrtos Beach being located within thin-bedded microcrystalline white carbonates (Figure 2), whereas the AVB samples were collected as clasts within the Neogene-Quaternary conglomerate, being a detrital input from carbonate strata (Figure 3).

Bulk mineral composition of six samples (MB1-3 and AVB1-3 from Myrtos and Avithos, respectively) was determined through X-ray powder diffraction (XRPD) analyses, using a Bruker D8 Advance diffractometer with Ni-filtered CuK α radiation, at 40 kV/40 mA with a ~2%–4% detection limit (Section of Earth Materials, University of Patras). Random powder mounts were pressed into the available holders. The specimens were scanned twice in the ranges of 3–70° and 17–24° 2 θ with a scanning angle step 0.015°/0.3 sec. and 0.015°/10 sec. respectively. The mineral phases were detected using the DIFFRACplus EVA 12[®] software

(Bruker-AXS, Billerica, MA, USA) based on the ICDD Powder Diffraction File of PDF-2 2006. Semi-quantitative analyses were performed based on the peak area calculations and using the same software and the “area” toolbox, while calculations of crystal sizes were carried out according to the Scherrer formula [33]. The petrographic examination of the collected samples was conducted on polished-thin sections using a polarizing microscope (Leica Microsystems, Leitz Wetzlar, Germany, Section of Earth Materials, University of Patras).

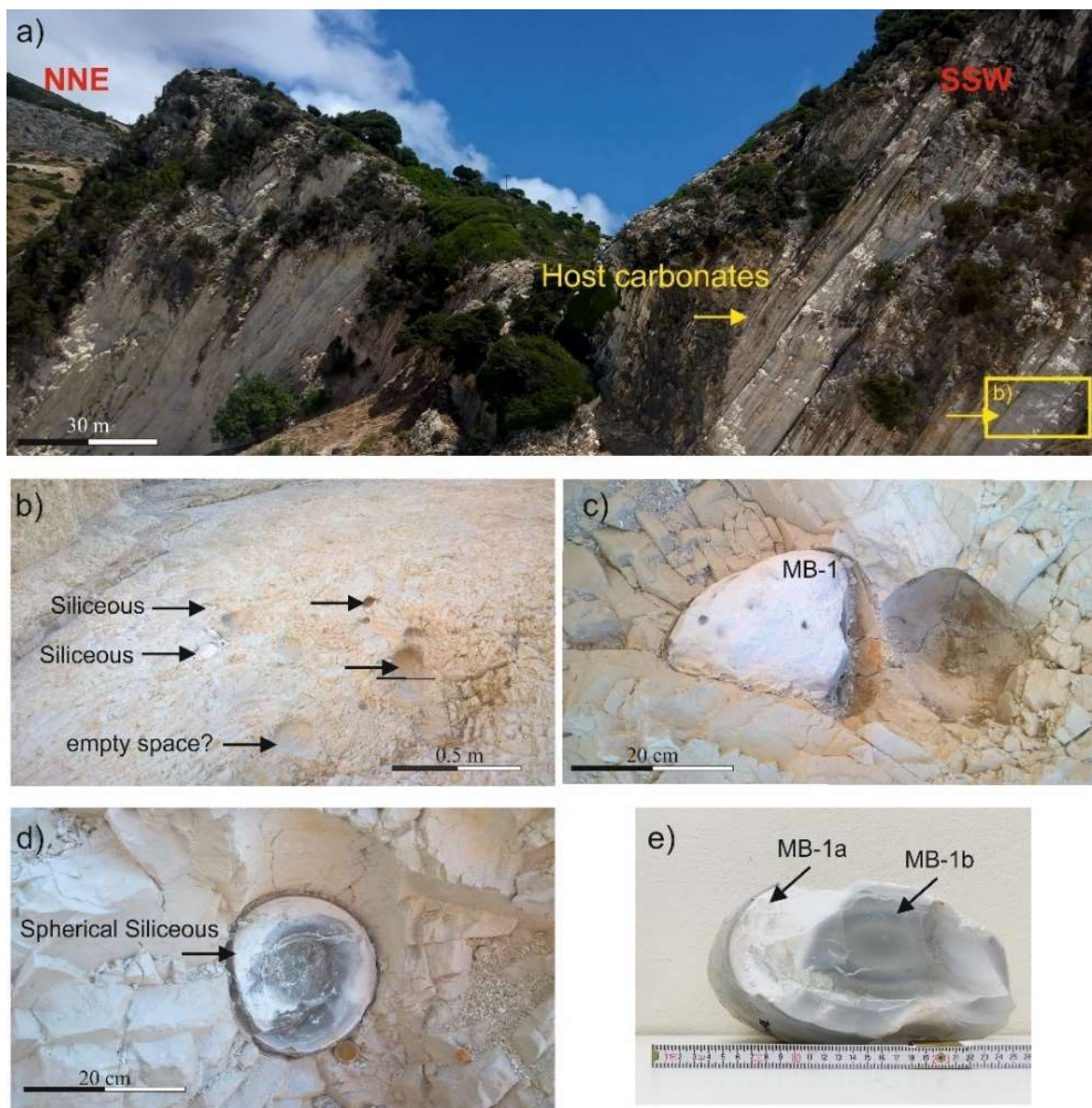


Figure 2. (a) Field view of the Myrtos Beach section; (b) MB sampling point with widespread siliceous subspherical nodules in carbonate strata; (c,d) detail view of in situ siliceous nodules; (e) macroscopic view of sample MB1.

A detailed observation of the microstructure and the distribution of silica was performed by Scanning Electron Microscopy (SEM). The thin sections were gold coated and were examined by a JEOL 6300 SEM at the Laboratory of Electron Microscopy and Microanalysis of the School of Natural Sciences, University of Patras. The SEM is equipped with an energy dispersive (ED) spectrometer and is operating under an accelerating voltage of 20 kV.

Transmission Electron Microscopy analysis was performed on the MB samples, in order to gain an insight into the variation in silica features between the outer rim (MB1a)

and the inner core (MB1b) of the nodule. The analyses were conducted on a JEOL JEM-2100 system at the School of Natural Sciences, University of Patras, operated at 200 kV (resolution: point 0.23 nm, lattice 0.14 nm). TEM Images and Selected Area Electron Diffraction (SAED) patterns were recorded by means of an Erlangshen CCD Camera (Gatan Model 782 ES500W). The selected specimens (MB1a, b) were prepared by dispersion in water and spread onto a carbon-coated copper grid (200 mesh).

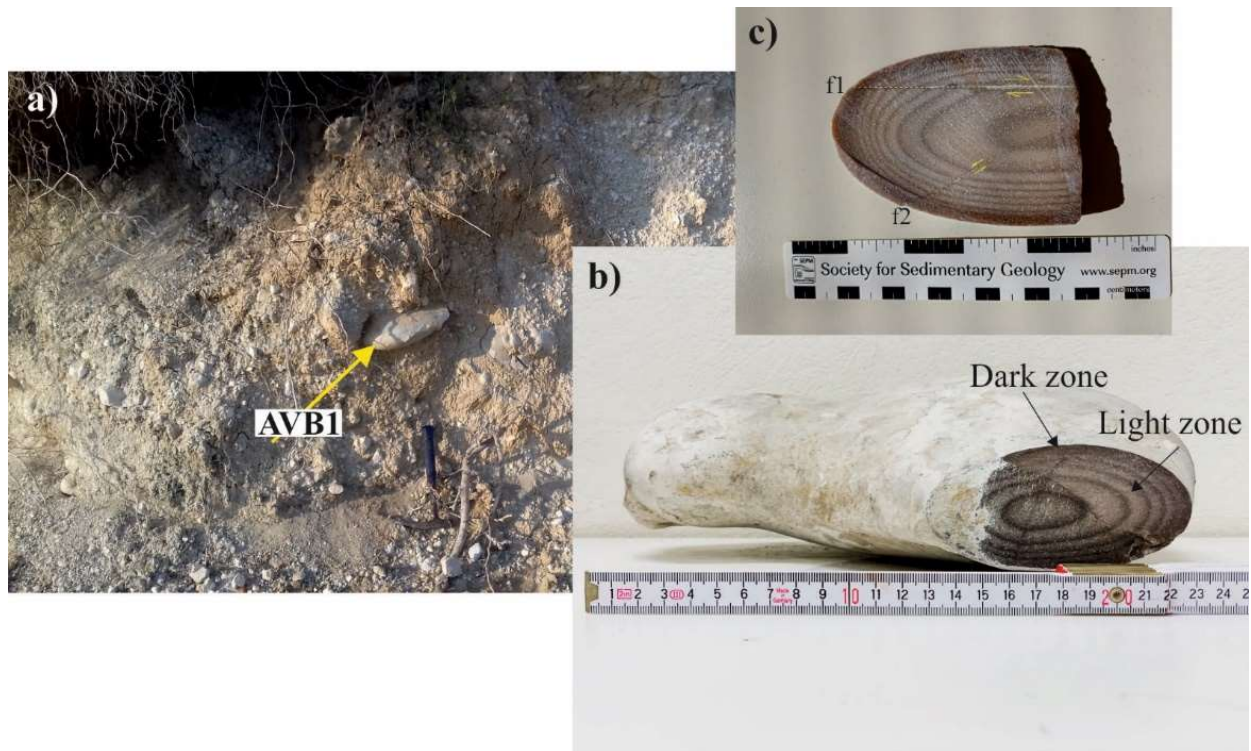


Figure 3. (a) Field view of the Avithos Beach sampling section; (b) macroscopic details of the AVB1 sample with the light/dark zonation and elliptical form; (c) detail of the nodule with microfaults (f1 and f2) occurrence.

Additionally, Raman spectra were collected from representative samples in order to detect the Si-bearing phases and complemented the TEM and XRD analysis. The examination was conducted using a Jobin-Yvon Horiba LabRam-HR Micro Raman spectrometer that is coupled with an Ar⁺ excitation source wavelength 514 nm and is equipped with an Olympus microscope (the 20× objective was used). The spectra were recorded within a 20 s acquisition time in the case of 10 successive spectral windows. The observation was conducted at the Laboratory of Electron Microscopy and Microanalysis of the University of Patras.

For determining the geochemical composition, one sample per site was examined through Wavelength Dispersive X-Ray Fluorescence (WD-XRF), in order to get the concentrations of major, minor and trace elements. The analysis was also carried out at the Laboratory of Electron Microscopy and Microanalysis of the University of Patras. An amount of 1.8 g of dried ground sample was mixed with 0.2 g of wax (acting as a binder) and was pressed on a base of boric acid to a circular powder pellet of 3.2 cm in diameter. Analyses were performed with a RIGAKU ZSX PRIMUS II spectrometer, which is equipped with Rh-anode running at 4 kW. Loss on ignition (LOI), as a measure of the volatile substances, was determined as weight loss during combustion at 950 °C for 2 h.

Thin sections were examined under an OPTIKA B293 optical microscope to identify and determine the microfauna and particularly the planktonic foraminifera.

4. Results

4.1. Macroscopic Lithological Features and Micropaleontological Findings

Macroscopic similarities and differences were observed among the sampled siliceous nodules from the two different localities (Table 1). In all hand rock samples a microcrystalline to cryptocrystalline texture with a conchoidal fracture and a hardness of 6.5–7 in Mohs scale were identified, while a distinct colour-zonation is recognized, with colours ranging from white to grey to beige grey.

Table 1. Macroscopic features and micropaleontological data of the studied siliceous nodules.

| Sample | AVB1 | MB1 |
|--------------------------------------|---|--|
| Colour (based on Munsell Chart) [32] | Light grey to pale yellow (2.5Y 7/1-6/1) with grey laminations (2.5Y 5/1) | Light grey (Gley 1 7N) |
| Texture of surface | rough | smooth |
| Cortex and alterations | Very thin | Alteration such as white patina of 5 mm to 1 cm |
| Shape of nodules | Elliptical | Subspherical |
| Identified fossils | Radiolaria— <i>Nasselaria</i> and <i>Spumelaria</i> , <i>Turborotalia cerroazulensis</i> , Algae, <i>Subbotina yeguaensis</i> , <i>Subbotina</i> sp., <i>Eorupertia</i> sp. | Radiolaria— <i>Nasselaria</i> and <i>Spumelaria</i> , <i>Globigerinelloides ferroensis</i> , <i>Alanlordella bentonensis</i> , <i>Hedbergella rishi</i> , <i>Hedbergella gorbachicae</i> , <i>Clavihedbergella</i> sp. |
| Inferred depositional setting | Proximal (toe of slope) | Distal (more pelagic) |

Collected nodules from Myrtos area (MB1 sample) are characterized by a dense, hard, grey-coloured body, with a sub-vitreous lustre covered with an outer white crust of a few centimeters in width exhibiting lower hardness than the inner grey part (Figure 2) and in some parts affected by red-brown metallic oxide precipitates. Moreover, the main body shows a concentric cryptocrystalline texture from the inner to the outer part of the core with slight variations in colour.

The AV1 sample displays also a distinct light/dark zonation (Figure 3), nevertheless it is rougher and coarser with a micro- rather than a cryptocrystalline texture, in comparison to the MB1 sample (Figure 3).

Through micro-paleontological analysis (Table 1), an Early Cretaceous age (Aptian-Albian) is implied for the MB1 sample, and a Late Eocene (Middle Bartonian-Priabonian) age for the AV1 (Table 1, Figure 4).

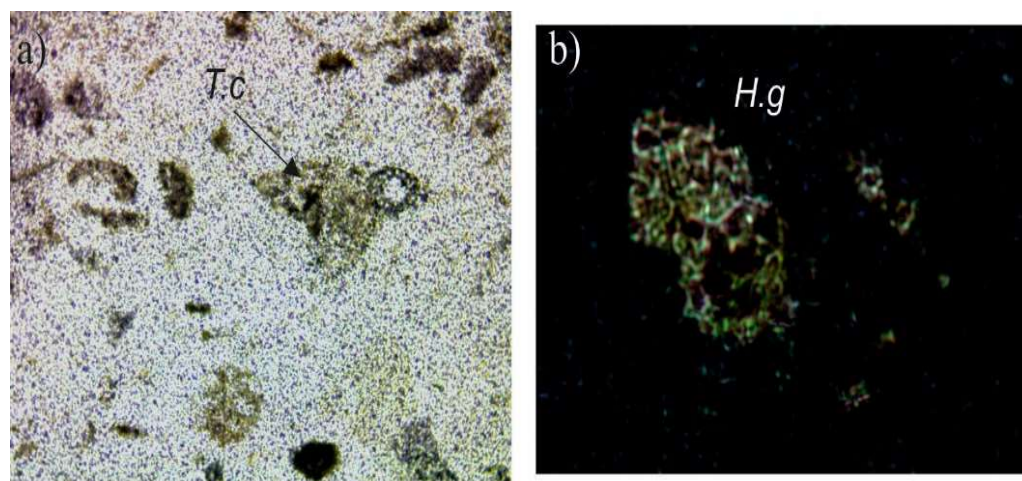


Figure 4. Photomicrographs of characteristic fossils in the studied samples: (a) *Turborotalia cerroazulensis* within a Si-rich matrix along with bioclast fragments in Avithos; (axial section $\times 100$); and (b) *Hedbergella gorbachicae* in Myrtos samples (axial section $\times 400$).

4.2. Mineralogical Composition

Representative semi-quantitative results and X-ray diffractograms of the studied samples are presented in Table 2 and Figure 5, respectively.

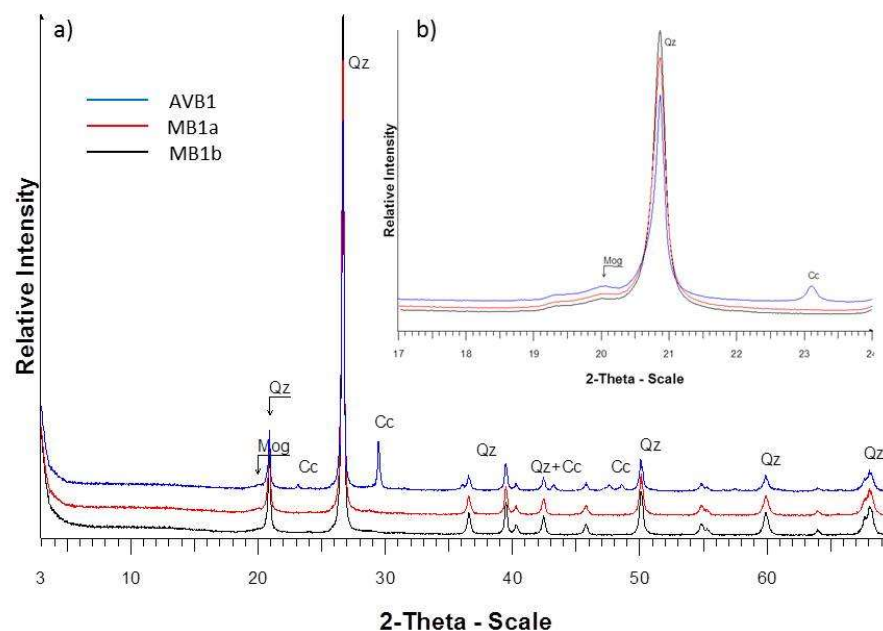


Figure 5. Representative diffractograms of the studied samples recorded in two different scanning areas: (a) Analysis of the bulk mineral compositions; and (b) Confirmation of the occurrence of moganite even in low amounts (Cc: Calcite; Mog: Moganite; Qz: Quartz).

Table 2. Semi quantitative analysis of mineral composition in studied samples (% crystalline phases).

| Sample | Calcite | Moganite | Quartz | Fe-Oxides |
|--------|---------|----------|--------|-----------|
| AVB1 | 13 | 3 | 84 | tr |
| MB1a | <2 | 2 | 95 | |
| MB1b | <2 | 2 | 95 | |

In the case of sample AVB1 (Figure 5) the major crystalline phase is, as expected, quartz (84 wt%) coexisting with low amounts of calcite (13 wt%). Moganite was also detected in minor amounts. Moreover, the high intensity and sharpness of X-ray diffraction peaks of quartz indicated its well crystalline character, while the X-ray diffractogram did not present any evidence of amorphous material in the matrix. According to the XRD analyses, the detected phases in MB-1a, b samples (Figure 5) consist predominantly of well crystalline quartz (95 wt%) with minor occurrences of moganite and traces of calcite. Based on the Scherrer formula calculations [33], the mean quartz particles size was 59, 37, and 40 nm, in AVB1, MB1a, and MB1b samples, respectively.

4.3. Optical Petrographic Features

The optical petrographical study under the polarizing microscope revealed that sample AVB1 is comprised of microcrystalline to cryptocrystalline siliceous material, filling the initial pores and acting as cement and/or replacing partially primary calcite and bioclasts (Figure 6). The syngenetically deposited grains or bioclasts usually retain their initial shape (“ghost crystals”) after being substituted by fine-grained quartz (Figure 6c). Locally spherulitic texture from radiating fibrous chalcedony with a diameter up to 300 μm was developed (Figure 6c,d), while microsparite was also observed. Frequent quartz crystals exhibit a drusy texture (Figure 6c), due to their different colours (white-grey to yellow). Additionally, the concentric textural characteristics observed in the microstructure of these rocks indicate selective replacement of micritic limestone from siliceous material

(Figure 6a,b). This mechanism led to the different ratios of silicate/carbonate minerals in different zones as is evident in the microscale observation.

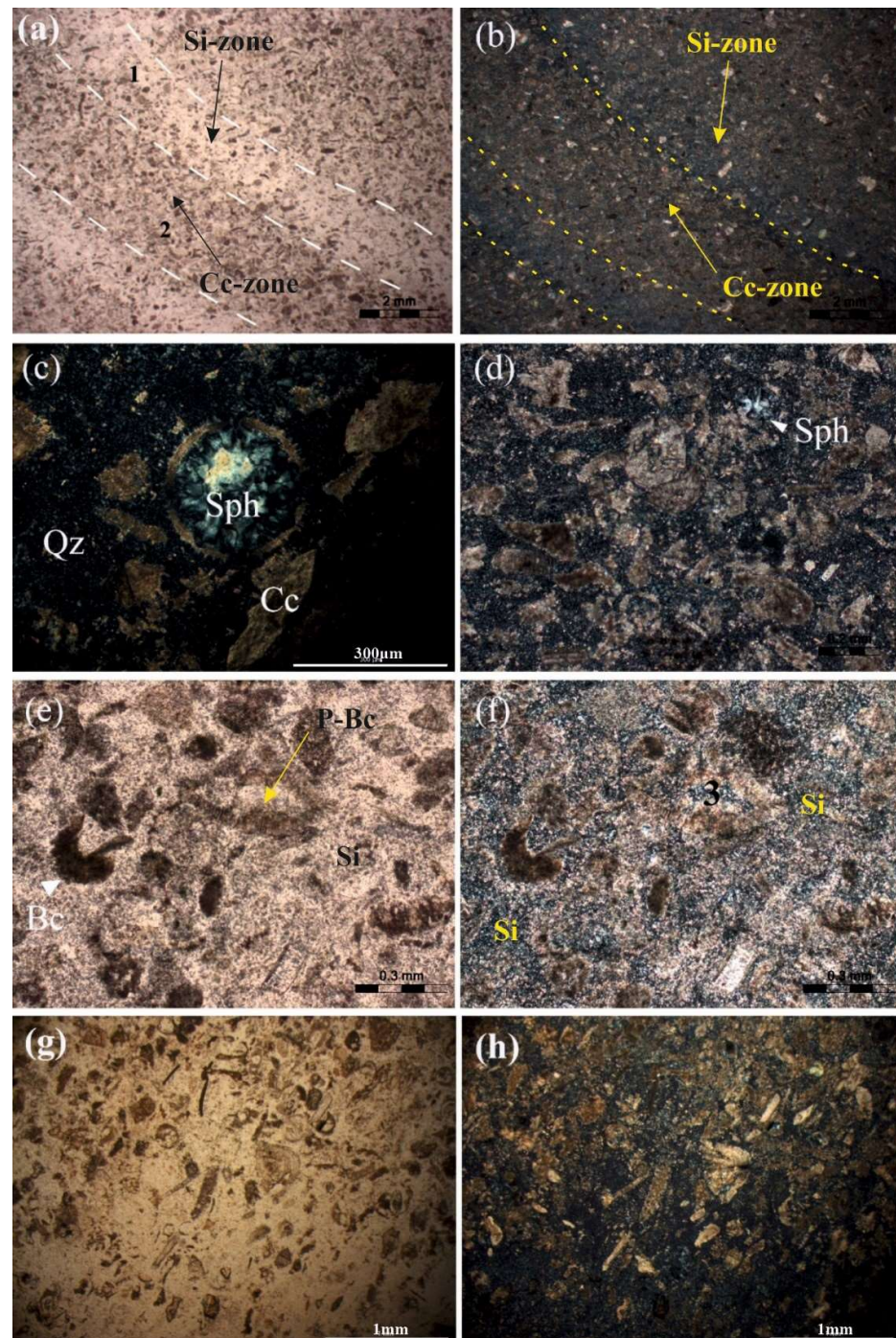


Figure 6. Photomicrographs of AVB1 microstructures in: (a,e) plane (PPL), and (b–d,f–h) cross polarized light (XPL); (a,b) characteristic concentric zoning of siliceous- (1, Si-zone) and carbonates (2, Cc)-rich phases; (c,d) spherulite of “ghost radiolarian” (Sph), quartz (Qz) and Calcite (Cc) within a siliceous-rich matrix; (e,h) bioclasts remnants (Bc), and micritic bioclasts partially replaced by siliceous material (P-Bc) within the matrix.

Samples MB-1a and 1b exhibit a finer and more homogenous siliceous texture compared to that in AVB1 (Figures 7 and 8). The MB samples comprise mainly microcrystalline to cryptocrystalline quartz acting as cement, with spherulites of chalcedony usually of smaller diameter compared to those in AVB1. Rare radiolarian and “ghost” calcareous

bioclasts are almost totally replaced by silica (Figure 7c). Significant texture variations between the main body and its rim were not distinguished, whilst the outer surface of these nodules (sample MB1a, Figure 7) exhibit a more cryptocrystalline texture compared to the main body (MB1b, Figure 8), locally with iron oxides (Figure 7c,d), as well as with a more porous matrix (Figure 9).

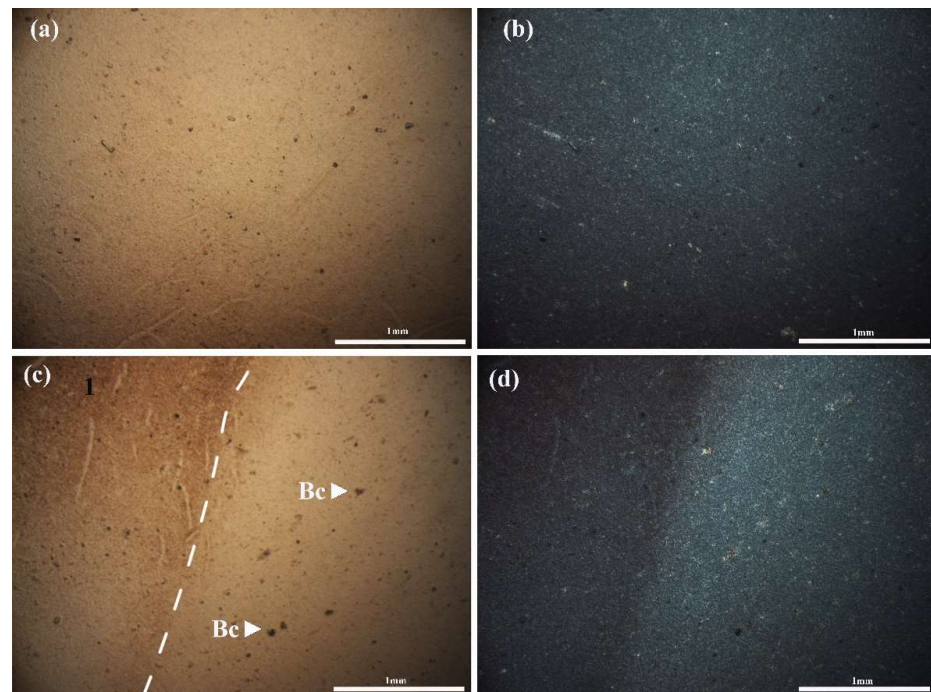


Figure 7. Photomicrographs of MB1a microstructures in (a,b) plane (PPL) and (c,d) cross polarized light (XPL) (Bc: bioclast, 1: micro-area impregnated with iron oxides).

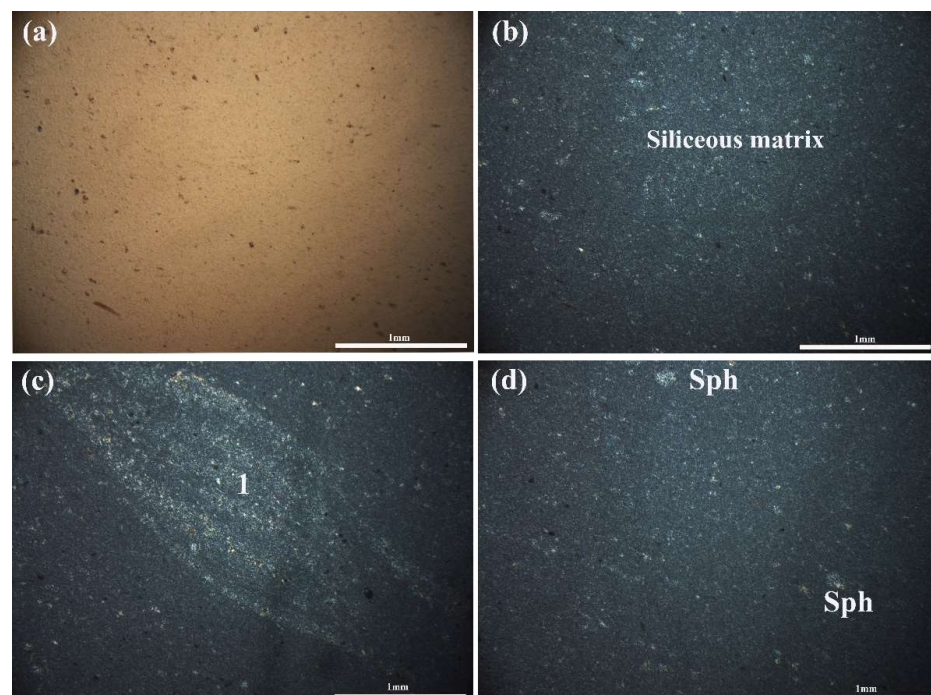


Figure 8. Photomicrographs of MB1b microstructures in (a) plane (PPL), and (b–d) cross polarized light (XPL) (Sph: spherulite, 1: micritic bioclast replaced by siliceous material).

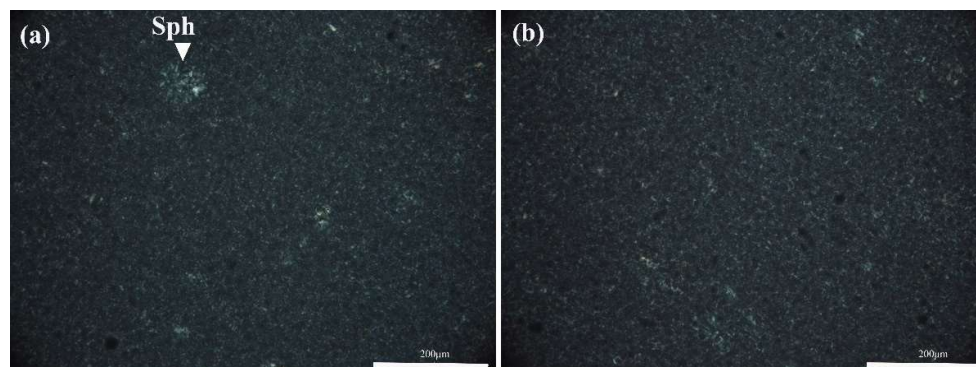


Figure 9. Photomicrographs in cross polarized light (XPL) comparing the textural characteristics of (a) inner part of nodule (MB1b); (b) a slightly more porous texture is evident for the outer surface (sample MB1a), (Sph: spherulite of a “ghost radiolarian”).

4.4. Scanning Electron Microscopy (SEM-EDS) and Transmission Electron Microscopy (TEM) Analysis

SEM-EDS analyses confirmed the optical petrographic examination. Representative Si, Ca elemental mapping analyses indicate that apart from the siliceous material in sample AVB1, there are significant calcium concentrations, representing the carbonates based on the petrographical results (Figure 10a–c). Moreover, scarce remnants of bioclasts were observed in the MB1a microstructure (Figure 10a), while recrystallized fibrous quartz commonly replaces carbonate bioclasts (Figure 11c,d).

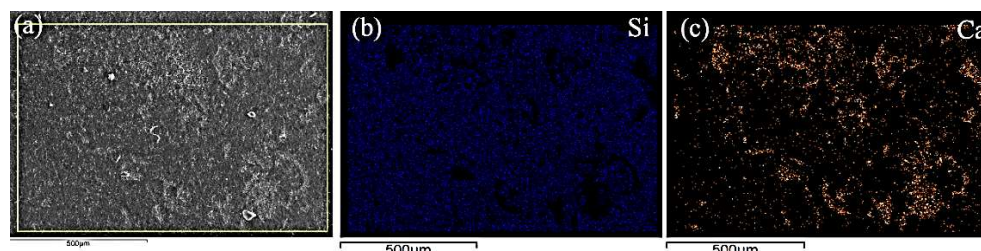


Figure 10. SEM-EDS elemental mapping of sample AVB1 indicating the mode of calcite enrichment: (a) view of the mapping area within the yellow rectangle; (b) distribution of Si; (c) distribution of Ca.

The study of samples MB1a and MB1b using a transmitted electron microscope (TEM) showed the nanometer and micrometer size of crystallites in the siliceous rock (Figure 12a,b). Crystallites of nano scale were observed mainly in sample MB1a, whereas both nano and micro crystallites were present in sample MB1b. Quartz crystallites were recognized in both samples as evidenced by all the strong diffractions $d = 3.3, 4.2, 2.4 \text{ \AA}$ (Figure 11a,b). Moganite was also recognized in the SAED of Figure 11 a by the diffraction $d = 3.1 \text{ \AA}$. TEM examination complemented XRD analysis confirming the presence of moganite in sample MB1.

4.5. Raman Spectroscopy Results

Micro-Raman spectroscopy was performed on samples MB1a, b and AVB1, and all the spectra were normalized based on the maximum intensity of each spectrum (Figure 13). The aim was to detect the silica polymorph moganite. A band at 464 cm^{-1} represents Si-O vibrations that are associated with quartz, whereas a band at 502 cm^{-1} is associated with moganite [34,35]. Moganite was detected in both samples with slight differences in peak areas and relative intensities in the spectra (Figure 13), especially in the case of sample MB1a. Specifically, the external surface-patina of MB1 (white area, MB1a) shows a broader peak area and lower peak intensity compared to samples MB1b and AVB1, being probably a result of lower content and/or lower crystallinity of the siliceous material within MB1a.

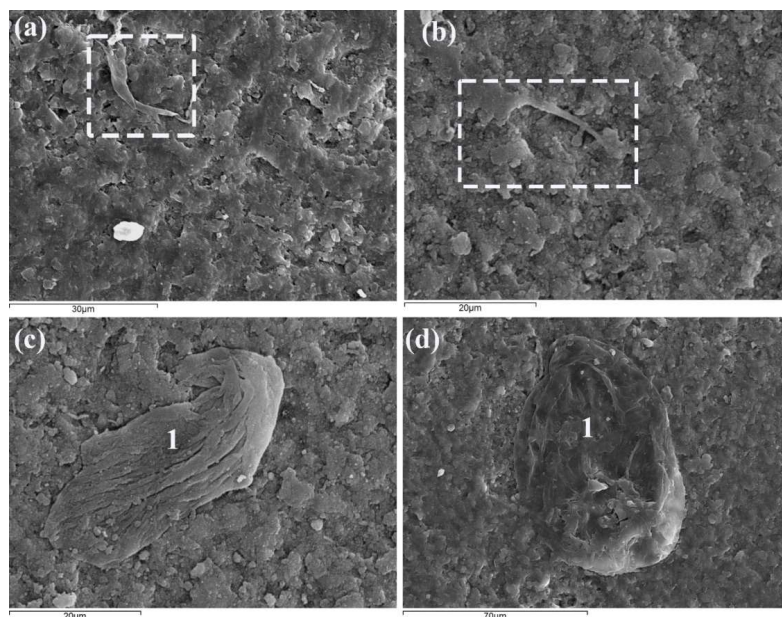


Figure 11. (a,b) Secondary electron image (SEI) in sample MB1a showing silicified bioclast remnants within the dotted boxes; (c,d) 1: siliceous bioclast fragments.

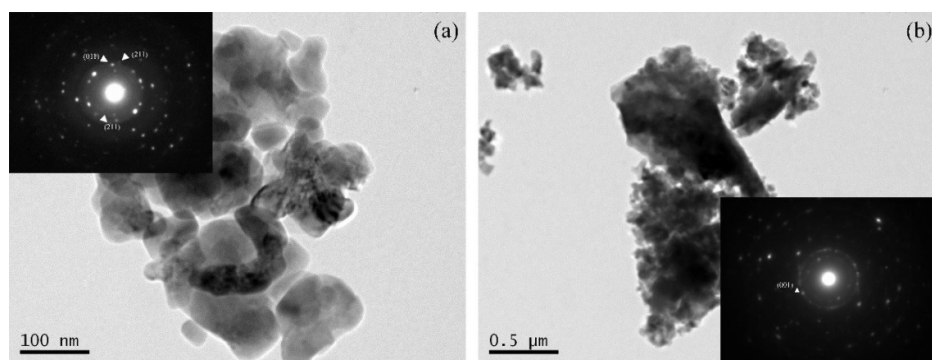


Figure 12. TEM photomicrographs: (a) quartz's and moganite's crystallites and reflections in SAED patterns (inset); and (b) quartz's crystallites and reflections in the SAED pattern (inset). Due to similarities in quartz and moganite d-spacings, there are not discrete moganite domains.

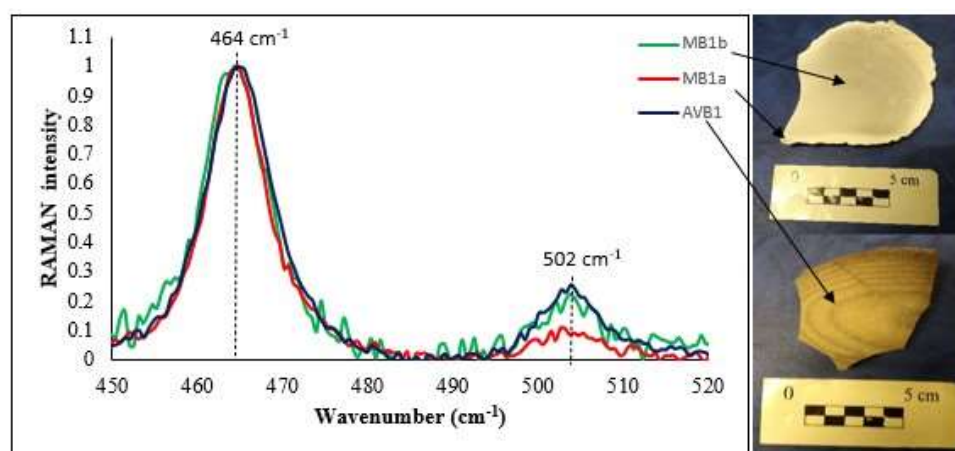


Figure 13. Raman spectra obtained by bulk samples. The labelled peaks at 464 cm^{-1} and 502 cm^{-1} are the bands of quartz and moganite. The picture on the right shows samples MB1 (top) and AVB1 (bottom), and the arrows display the areas where the spectra were obtained.

4.6. Geochemical Features

Representative chemical analyses of the studied samples are presented in Table 3. Results from sample AVB1 indicate that its bulk composition is comprised mainly of silicon oxide (87 wt%), lower amounts of calcium oxide (6 wt%) and traces (<0.5 wt%) of other oxides and elements. The loss on ignition (LOI) was determined at 7.16 wt% and after combination with the aforementioned mineralogical results, it could be principally attributed to the carbonates and with small amounts to hydrated amorphous or semi-crystalline silica-rich phases. The latter phases could not be detected using XRD, as they occur in concentrations below the detection limit and/or their crystallinity could not be resolved (Figure 5).

Table 3. Representative chemical analyses of the studied samples.

| Oxides wt% | AVB1 | MB1a | MB1b | Elements mg/kg | AVB1 | MB1a | MB1b |
|---|---------------|--------------|---------------|-------------------|------|------|------|
| SiO ₂ | 87.40 | 98.30 | 98.70 | Cr | 18 | 15 | 22 |
| TiO ₂ | 0.02 | 0.02 | 0.02 | Co | 154 | 68 | 67 |
| Al ₂ O ₃ | <0.01 | 0.05 | <0.01 | Ni | <1 | 3 | 3 |
| Fe ₂ O ₃ ^t | 0.03 | 0.01 | 0.01 | Cu | 21 | 15 | 8 |
| MnO | 0.01 | 0.01 | 0.01 | Zn | 10 | 7 | 8 |
| MgO | 0.29 | 0.13 | 0.10 | Rb | <1 | <1 | <1 |
| CaO | 6.17 | 0.15 | 0.14 | Sr | 56 | 6 | 5 |
| Na ₂ O | 0.10 | 0.11 | 0.12 | Y | <1 | <1 | <1 |
| K ₂ O | 0.02 | 0.03 | 0.03 | Zr | 2 | <1 | <1 |
| P ₂ O ₅ | 0.01 | 0.02 | 0.01 | Nb | <1 | 5 | 29 |
| LOI | 7.16 | 0.91 | 1.16 | Pb | 20 | 25 | 18 |
| Total | 101.22 | 99.74 | 100.31 | Ba | 14 | <1 | <1 |
| | | | | V | 23 | 24 | 24 |
| | | | | Hf | <1 | <1 | <1 |
| | | | | S | <1 | 3 | 555 |

Siliceous nodules from Myrtos area (MB1a, b) have high purity siliceous materials (containing 98.26–98.67 wt% SiO₂) with minor occurrences of other oxides and trace elements in their matrix, in accordance with the petrographic and mineralogical results. The LOI values are much lower (0.91–1.16 wt%) compared to that in sample AVB1 and related mainly to minor carbonates and silica-rich hydrated material. The rims of sample MB1 (MB1a) exhibited a higher LOI value compared to its body. Among the trace elements, only sulfur in sample MB1b exhibited values above 200 ppm, whereas Sr displays elevated values in sample AV1, probably related to the high content of Ca in carbonate remnants.

5. Discussion: Formation of the Nodules and Their Diagenesis

The studied siliceous nodules from Myrtos and Avithos beaches in Kefalonia Island display characteristic concentric textures both at macroscopic and microscopic scale, being more evident in samples from Avithos beach. In general, the analyzed nodules from both locations display a dense fine-grained siliceous sedimentary fabric, composed mainly of microcrystalline or cryptocrystalline quartz with rare to common residual calcite. These characteristics are similar to the features of the siliceous concretions from Ionian Islands described by Bourli et al. [4], although in our case the micro-zoning is more evident. Siliceous Radiolaria and other bioclasts in the microstructures of the nodules reflect the biogenic source of silica.

The principle textural characteristics of the studied nodules, namely the grain size and the concentric zoning, are attributed to the very early burial (early epigenetic) stage and/or diagenetic conditions of formation [7,36,37]. During the early epigenetic phase, the major factors include the physicochemical conditions below the seabed (i.e., redox potential) that control silica dissolution and precipitation, any bioturbation activity and the textural characteristics of the surrounding calcareous muds. In later diagenetic stages, the major factors include the textural characteristics of the host rocks, including porosity,

any tectonic activity resulting in fracturing, as well as circulation of diagenetic and/or hydrothermal/geothermal fluids.

Generally, moganite, being a polymorph of SiO_2 , is used as a diagenetic index, since it is considered a moderate phase of amorphous to the microcrystalline quartz formation [9,10,38]. Therefore, the occurrence of moganite in the studied samples implies that biogenetic amorphous silica was initially precipitated, and almost totally recrystallized later as the degree of diagenesis increased [3]. Therefore, the amount and or the crystallinity of moganite, as well as the formation of crystalline quartz at the expense of moganite and amorphous phases, are measures of compaction during burial and/or effects of circulated diagenetic/hydrothermal solutions, as well as tectonic impacts. The moganite content of the studied samples, using the work of Graetsch and Grünberg [39], indicates an approximate age of formation of ~150 Ma. This age is in accordance with the depositional age of the Lower Cretaceous Myrtos samples, but the Avithos samples are much younger (Eocene); therefore an additional impact apart from the normal burial history is implied for Avithos siliceous nodules.

In order to elucidate the depositional environment, certain geochemical proxies are applied. Based on the relative concentrations of silica, aluminum and iron oxides [40] it is suggested that the depositional setting was a continental margin (Figure 14a). Moreover, the diagram proposed by Adachi et al. [41] (Figure 14b) suggests a hydrothermal impact; nevertheless, both in Pre-Apulian and Ionian Units no magmatic activities have been reported, hence in our case it is more appropriate to accept the influence of diagenetic (geothermal) fluids.

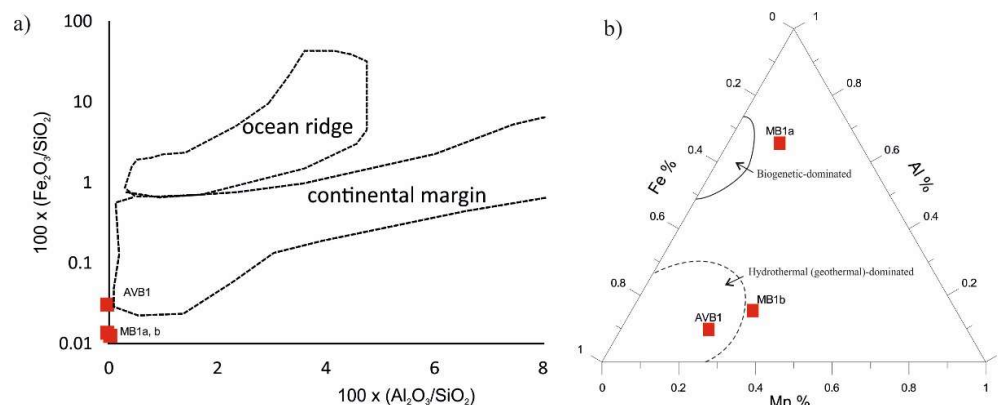


Figure 14. (a) Scatter plot of silicon, iron, aluminum oxides ratios (modified after Murray 1994 [40]); (b) Ternary plot of Al-Fe-Mn % in the studied samples (modified after Adachi et al. [41]).

5.1. Myrtos Siliceous Nodules

Based on the remaining bioclasts within the matrix of the nodules, the Myrtos nodule is of Early Cretaceous age, hosted within thin-bedded microcrystalline limestones, which were formed in a pelagic relatively deep-water environment. The MB nodules are composed almost entirely of siliceous material (mainly quartz) reflecting a Si-rich palaeoenvironment, as well as Si-precipitation under relatively stable physicochemical conditions (Gotze et al., 2021) at the early epigenetic stage shortly after burial [40]. The high silica content in such conditions can probably be explained by the higher solubility of calcium ions acting as electrolytes, in comparison to Si; this Ca^{2+} saturation of the solution is reflected by the deposition of pure micritic limestone, acting as host rocks. This process favoured the observed advanced silicification [42] in Myrtos, evidenced by the appearance of “ghost” radiolarian and calcareous bioclasts being totally replaced by silica.

An interesting feature of the Myrtos nodules is the younger outer white siliceous crust (MB1a, Figure 3), which exhibits lower hardness, as well as smaller size of quartz crystals compared to the main body (M1Ab). The formation of this crust is related to the occurrence of bioclast remnants that were resistant to silicification (Figures 11 and 14b) [42]. Alternatively, it may be the result of frictional activity at the interface of the nodule and the

host rock. Additionally, the minor occurrence of opaque minerals in micro-areas of the MB matrix may be associated with diagenetic solutions circulation during the episode of rim precipitation and/or the result of weathering contributing further to a loose structure [12].

Moreover, the size of the spherulites (up to 200 μm) can be attributed to the host porosity and/or the size of the grains replaced in the host rock [42]. The primary porosity of the host rock seems to influence the final size and shape of the siliceous nodules; Pelagic limestones like the Lower Cretaceous in Myrtos have low porosity that might have contributed to the observed well-formed sub-spherical and spherical nodules during diagenesis.

5.2. Avithos Siliceous Nodules

The studied nodules from Avithos contain bioclasts that point to the Eocene age. Since the published geological map of the area does not show Cenozoic carbonate strata in the vicinity of Avithos it is safe to assume that either the local stratigraphy is not well documented, or that the nodules represent lithologies of the Eocene of the Ionian Unit developing in the eastern part of Kefalonia island (see Figure 1) and have been transported for a long distance (i.e., allochthonous); actually, as described in the sampling section, the studied AVB nodules were retrieved from a Neogene-Quaternary conglomerate.

The nature of the bioclasts from Avithos represents a shallow shelf or toe of slope environment, in which the sedimentation regime was influenced by both chemical precipitation and detrital influx.

The texture of the AVB nodules shows selective replacement of primary carbonates by siliceous material; nevertheless, the frequent remnants of calcite, indicate more variable physicochemical conditions than in Myrtos case, as well as on the silica supply during the period of precipitation. Moreover, in the case of AVB1 siliceous nodule, in which calcite has remained, Sr was also not totally mobilized to the host rocks. The larger size of the spherulites (up to 300 μm) of the nodules are probably attributed to a larger porosity of the host rock [37]. Nevertheless, additional factors that could play a significant role include the tectonic activity, in combination to the circulation of geothermal or diagenetic fluids. The epigenetic tectonic impact is more evident in the Avithos nodules, as the microfaulting indicates, promoting additionally the secondary porosity [43]; this more evident impact can either be related to the intensity of the tectonism, and/or to the calcite impurities within the nodules that reduce the mechanical strength.

In terms of diagenetic imprint, the presented data, particularly of the quartz and moganite relative concentrations and crystallinity, suggest that the Avithos nodules display larger crystals of quartz, as well as higher crystallinity of moganite (Figure 13) than the nodules in Myrtos. Hence, although younger in age than Myrtos, Avithos nodules seem to have experienced higher degree of diagenesis, possibly related to a combination of other factors, such as tectonic and geothermal impacts.

6. Conclusions

This research work involves a first attempt to study the characteristics of siliceous nodules hosted within carbonates that outcrop in Myrtos and Avithos beaches, in the western coastal part of Kefalonia Island, in Greece. The objectives of the study focus on the textural and compositional features of the siliceous rocks by applying a set of optical and electronic microscopical techniques, mineralogical and geochemical analyses. The main conclusions of this study are summarized below:

- In Myrtos and Avithos beaches concentric spherical and elliptical siliceous nodules occur, respectively.
- Myrtos nodules formed in a more distal and deeper palaeoenvironment than the Avithos ones.
- The presence of moganite in both sites suggests an amorphous silica precursor of biogenic origin such as from Radiolaria.

- The Lower Cretaceous Myrtilos siliceous (flint-like) nodules exhibit higher siliceous purity than the Eocene Avithos nodules, which contain significant calcite residue.
- However, the obtained data indicate a higher degree of recrystallization for the siliceous nodules in Avithos than in Myrtilos, probably related to the circulation of diagenetic fluids along tectonic fractures.
- The distribution of Al-Fe-Mn provides additional evidence for a geothermal-related imprint in Avithos nodules.
- Thorough studies of siliceous nodules provide a more comprehensive understanding of the respective sedimentary formation conditions, as well as the diagenetic pathways.

Author Contributions: Conceptualization, M.W.-K. and S.K.; Investigation, P.L., V.X., M.W.-K., P.P., G.I., E.Z. and S.K.; Methodology, P.L., V.X., M.W.-K., P.P. and G.I.; Software, S.K.; Supervision, S.K.; Validation, P.L., M.W.-K. and S.K.; Writing—original draft, P.L., P.P. and S.K.; Writing—review and editing, V.X., M.W.-K., E.Z., G.I. and S.K. All authors have read and agreed to the published version of the manuscript.

Funding: This research received no external funding.

Data Availability Statement: The data presented in this review study are available on request from the corresponding author.

Acknowledgments: The authors would like to thank the Laboratory of Electron Microscopy and Microanalysis, Faculty of Natural Sciences, University of Patras. Panagiotis Balasis of Sample Preparation and Thin Section Laboratory is acknowledged for supporting sample preparation. Additionally, Geologist Maria Kalpogiannaki is thanked for technical assistance in GIS, as well as two anonymous reviewers, and Georgia Pe-Piper are gratefully acknowledged for their valuable comments during the review stage.

Conflicts of Interest: The authors declare no conflict of interest.

References

1. Hesse, R. Origin of chert: Diagenesis of biogenic siliceous sediments. *Geosci. Can.* **1988**, *15*, 171–192.
2. Bohrman, G.; Abelman, A.; Gersonde, R.; Hubberten, H.; Kuhn, G. Pure siliceous ooze, a diagenetic environment for early chert formation. *Geology* **1994**, *22*, 207–210. [[CrossRef](#)]
3. Bourli, N.; Kokkaliari, M.; Iliopoulos, I.; Pe-Piper, G.; Piper, D.J.W.; Maravelis, A.G.; Zelilidis, A. Mineralogy of siliceous concretions, cretaceous of Ionian zone, western Greece: Implication for diagenesis and porosity. *Mar. Pet. Geol.* **2019**, *105*, 45–63. [[CrossRef](#)]
4. Bourli, N.; Kokkaliari, M.; Dimopoulos, N.; Iliopoulos, I.; Zoumpouli, E.; Iliopoulos, G.; Zelilidis, A. Comparison between Siliceous Concretions from the Ionian Basin and the Apulian Platform Margins (Pre-Apulian Zone), Western Greece: Implication of Differential Diagenesis on Nodules Evolution. *Minerals* **2021**, *11*, 890. [[CrossRef](#)]
5. Abrajvitch, A. Diagenetic formation of bedded chert: Implications from a rock magnetic study of siliceous precursor sediments. *Earth Planet. Sci. Lett.* **2020**, *533*, 116039. [[CrossRef](#)]
6. Chatzimpaloglou, P. A geoarchaeological methodology for sourcing chert artefacts in the Mediterranean region: A case study from Neolithic Skorba on Malta. *Geoarchaeology* **2020**, *35*, 897–920. [[CrossRef](#)]
7. Raviolo, M.M.; Barbosa, A.J.A.; Neumann, V.H. Characteristics, distribution and diagenetic stages of chert in the La Silla Formation (Lower Ordovician), Argentine Precordillera. *Ann. Acad. Bras. Ciências* **2009**, *81*, 781–792. [[CrossRef](#)]
8. Pope, M. Cherty carbonate facies of the Montoya Group, southern New Mexico and western Texas and its regional correlatives: A record of Late Ordovician paleoceanography on southern Laurentia. *Palaeogeogr. Palaeoclimatol. Palaeoecol.* **2004**, *210*, 367–384. [[CrossRef](#)]
9. Ye, Y.; Frings, P.J.; Blanckenburg, F.; Feng, Q. Silicon isotopes reveal a decline in oceanic dissolved silicon driven by biosilicification: A prerequisite for the Cambrian Explosion? *Earth Planet. Sci. Lett.* **2021**, *566*, 116959. [[CrossRef](#)]
10. Zhang, M.; Moxon, T. Infrared absorption spectroscopy of SiO₂-moganite. *Am. Mineral.* **2014**, *99*, 671–680. [[CrossRef](#)]
11. Götze, J.; Stanek, K.; Orozco, G.; Liesegang, M.; Mohr-Westheide, T. Occurrence and Distribution of Moganite and Opal-CT in Agates from Paleocene/Eocene Tuffs, El Picado (Cuba). *Minerals* **2021**, *11*, 531. [[CrossRef](#)]
12. Luedtke, B.E. *An Archaeologist's Guide to Chert and Flint*, UCLA Cotsen Institute of Archaeology Press, Archaeological Research Tools; Institute of Archaeology University of California: Los Angeles, CA, USA, 1992; pp. 1–154. ISBN 0-917956-75-3.
13. Cackler, P.R.; Glascock, M.D.; Neff, H.; Chiarulli, B.M. Effects of weathering on the coloration of chert and its implications for provenance studies. *Lithic Technol.* **1999**, *24*, 81–90. [[CrossRef](#)]
14. Moník, M.; Nerudová, Z.; Schnabl, P. Investigation of heat-treated artefacts from Pleistocene sites. *J. Archaeol. Sci. Rep.* **2021**, *37*, 102920. [[CrossRef](#)]

15. Lampropoulou, P.; Laskaris, N.; Petrounias, P.; Giannakopoulou, P.P.; Rogkala, A.; Kalampounias, A.G.; Tsigrou, P.; Katagas, C.G.; Iliopoulos, I. Petrogeochemical approaches to the characterization of obsidian derived from Nychia area (Milos Island, Greece) using combined methods. *Microchem. J.* **2020**, *156*, 104843. [[CrossRef](#)]
16. Biagi, P.; Nisbet, R.; Michniak, R. The Chert Outcrops of the Pindus Range of Western Macedonia (Greece) and their Middle Palaeolithic Exploitation. *Quarry* **2015**, *11*, 3–16.
17. Magganas, A.; Galanidou, N.; Chatzimpaloglou, P.; Kati, M.; Iliopoulos, G.; Katerinopoulos, A. Petrology and Provenance of Lithic Raw Materials used to knap stone: A Case Study from the Inner Ionian Sea. *Bull. Geol. Soc. Greece* **2018**, *53*, 277–298. [[CrossRef](#)]
18. Pe-Piper, G.; Piper, D.J.W.; Bourli, N.; Zelilidis, A. Evolution of Sedimentary Basins as Recorded in Silica Concretions: An Example from the Ionian Zone, Western Greece. *Minerals* **2021**, *11*, 763. [[CrossRef](#)]
19. Bergmann, H.; Braune, K.; Dremel, G.; Hatzopoulos, E.; Hug, F.; Uliczny, E. *Geological Map of Greece, Cephalonia Island Sheet, 1:50,000*; IGME: Athens, Greece, 1968.
20. Underhill, J.R. Late Cenozoic deformation of the Hellenide foreland, Western Greece. *Geol. Soc. Am. Bull.* **1989**, *101*, 613–634. [[CrossRef](#)]
21. Accordi, G.; Carbone, F. *Lithofacies Map of Hellenide Pre-Apulia Zone (Ionian Island, Greece)*; Centro di Studio per la Geologia dell'Italia Centrale; CNR: Roma, Italy, 1992.
22. Accordi, G.; Carbone, F.; Di Carlo, M.; Pignatti, J. Microfacies analysis of deep-water breccias clasts: A tool for interpreting shallow-vs. deep-ramp Paleogene sedimentation in Cephalonia and Zakynthos (Ionian Islands, Greece). *Facies* **2014**, *60*, 445–466. [[CrossRef](#)]
23. Zelilidis, A.; Kontopoulos, N.; Piper, D.J.W.; Avramidis, P. tectonic and sedimentological evolution of the Pliocene—Quaternary basins of Zakynthos Island, Greece: Case study of the transition from compressional to extensional tectonics. *Basin Res.* **1998**, *10*, 393–408. [[CrossRef](#)]
24. Aubouin, J. Zone preapulienne et zone du Gavrovo en Peloponnese occidentale. *Bull. Soc. Geol. Fr.* **1962**, *4*, 785–794. [[CrossRef](#)]
25. Jenkyns, D.A.L. Structural development of western Greece. *Am. Assoc. Pet. Geol. Bull.* **1972**, *56*, 128–149.
26. Smith, A.G.; Moores, E.M. Hellenides. In *Mesozoic and Cenozoic Orogenic Belts*; Spencer, A.M., Ed.; Scottish Academic Press: Edinburg, UK, 1974; pp. 159–186.
27. Jones, W.D.V. Results of recent geological surveys in central-western Greece. *Proc. Geol. Soc. Lond.* **1968**, *1645*, 306–310.
28. British Petroleum Co Ltd. The geological results of petroleum exploration in western Greece. *Inst. Geol. Subsurf. Res.* **1971**, *10*, 1–73.
29. Karakitsios, V. Western Greece and Ionian Sea petroleum systems. *AAPG Bull.* **2013**, *97*, 1567–1595. [[CrossRef](#)]
30. Zelilidis, A.; Maravelis, A.G.; Tserolas, P.; Konstantopoulos, P.A. An overview of the petroleum systems in the Ionian zone, onshore NW Greece and Albania. *J. Petrol. Geol.* **2015**, *38*, 331–348. [[CrossRef](#)]
31. Karakitsios, V.; Rigakis, N. Evolution and petroleum potential of western Greece. *J. Petrol. Geol.* **2007**, *30*, 197–218. [[CrossRef](#)]
32. *Munsell Soil Color Charts (Year 2000 Revised Washable Edition)*; Munsell Color Company—X-Rite: New Windsor, NY, USA, 2000; 50p.
33. Patterson, A. The Scherrer Formula for X-Ray Particle Size Determination. *Phys. Rev.* **1939**, *56*, 978–982. [[CrossRef](#)]
34. Etchepare, J.; Merian, M.; Smetankine, L. Vibrational normal modes of SiO₂. I. a and b quartz. *J. Phys. Chem.* **1974**, *60*, 1873–1876. [[CrossRef](#)]
35. Sato, R.K.; McMillan, P.F. An infrared and Raman study of the isotopic species of a-quartz. *J. Phys. Chem.* **1987**, *91*, 3494–3498. [[CrossRef](#)]
36. Madsen, H.B.; Stemmerik, L. Diagenesis of Flint and Porcellanite in the Maastrichtian Chalk at Stevns Klint, Denmark. *J. Sediment. Res.* **2010**, *80*, 578–588. [[CrossRef](#)]
37. Lawrence, M.J.F. Sedimentology and petrography of early diagenetic chert and dolomite in the Late Cretaceous-early Tertiary Amuri Limestone Group, eastern Marlborough, New Zealand. *N. Z. J. Geol. Geophys.* **1993**, *36*, 9–25. [[CrossRef](#)]
38. Schmidt, P.; Bellot-Gurlet, L.; Lea, V.; Sciau, P. Moganite detection in silica rocks using Raman and infrared spectroscopy. *Eur. J. Mineral.* **2013**, *25*, 797–805. [[CrossRef](#)]
39. Graetsch, H.A.; Grünenberg, J.M. Microstructure of flint and other chert raw materials. *Archaeometry* **2012**, *54*, 18–36. [[CrossRef](#)]
40. Murray, W.R. Chemical criteria to identify the depositional environment of chert: General principles and applications. *Sediment. Geol.* **1994**, *90*, 213–232. [[CrossRef](#)]
41. Adachi, M.; Yamamoto, K.; Sugisaki, R. Hydrothermal chert and associated siliceous rocks from the northern Pacific their geological significance as indication of ocean ridge activity. *Sediment. Geol.* **1986**, *47*, 125–148. [[CrossRef](#)]
42. Siever, R. Sedimentological consequences of a steady-state ocean-atmosphere. *Sedimentology* **1968**, *11*, 5–29. [[CrossRef](#)]
43. Spence, G.H.; Finch, E. Influences of nodular chert rhythmites on natural fracture networks in carbonates: An outcrop and two-dimensional discrete element modelling study. In *Advances in the Study of Fractured Reservoirs*; Spence, G.H., Redfern, J., Aguilera, R., Bevan, T.G., Cosgrove, J.W., Couples, G.D., Daniel, J.-M., Eds.; Special Publications; Geological Society: London, UK, 2015; Volume 374, pp. 211–249.